

## Stable perovskite based photodetector in impedance and capacitance mode

Tahseen A. Qasuria<sup>a</sup>, Shahid Alam<sup>a</sup>, Khasan S. Karimov<sup>a,b</sup>, Noshin Fatima<sup>a,c,\*</sup>, Yahya S. Alharthi<sup>d</sup>, Hamad F. Alharbi<sup>e</sup>, Nabeel H. Alharthi<sup>f</sup>, N. Amin<sup>g</sup>, Md. Akhtaruzzaman<sup>c,h,\*</sup>

<sup>a</sup> Ghulam Ishaq Khan Institute of Engineering Sciences and Technology, Topi 23640, KPK, Pakistan

<sup>b</sup> Center for Innovative Development of Science and Technologies of Academy of Sciences, Rudaki Ave., 33, Dushanbe 734025, Tajikistan

<sup>c</sup> Solar Energy Research Institute, The National University of Malaysia, 43600 Bangi, Selangor, Malaysia

<sup>d</sup> Department of Electrical Engineering, King Saud University, Riyadh 11421, Saudi Arabia

<sup>e</sup> Department of Mechanical Engineering, College of Engineering, King Saud University, Riyadh 11421, Saudi Arabia

<sup>f</sup> Center of Excellence for Research in Engineering Materials, King Saud University, Riyadh 11421, Saudi Arabia

<sup>g</sup> Institute of Sustainable Energy, Universiti Tenaga Nasional (@The National Energy University), Jalan IKRAM-UNITEN, 43000 Kajang, Selangor, Malaysia

<sup>h</sup> INTEGRA, FKAB, Universiti Kebangsaan Malaysia (UKM), 43600 Bangi, Selangor, Malaysia

### ARTICLE INFO

#### Keywords:

Perovskite  
Photodetector  
Frequency  
Hybrid organic-inorganic  
Impedance mode  
Capacitance mode

### ABSTRACT

Nowadays perovskite emerges as a promising photosensitive material for next-generation solution-processed devices. Perovskite-based solar cells degrade in ambient conditions up to some extent, after which they are discarded. In our work, we are using reusing the degraded cells as a high-performance stable perovskite-based photodetector. The symmetry of the detector is FTO/PEDOT:PSS/Perovskite/PC<sub>61</sub>BM/CdS/Ag showing sensitivity to light with respect to (w.r.t) impedance and capacitance. To enhance the excitons generation and absorption of light, the electron transport layer of cadmium sulfide along with PC<sub>61</sub>BM is selected and PEDOT:PSS layer is used for hole transportation. Atomic force microscopy, X-ray diffraction, and UV-absorption spectrum were obtained to study the surface morphology, composition, and absorption of the perovskite layer. The electric parameters within the frequency range 100 Hz to 200 kHz of samples under the effect of light were investigated. Experimental results showed that with the change in light intensity from dark to 325 W/m<sup>2</sup>, the highest impedance and capacitance were observed at 100 Hz. The impedance sensitivity is  $-126.154 \text{ k}\Omega \text{ m}^2/\text{W}$  and the uppermost capacitance sensitivity w.r.t light intensity is  $6.77 \text{ pF m}^2/\text{W}$ . Frequency-impedance and capacitance relationships and sensitivities were also measured. The results showed that in the range from 100 Hz to 200 kHz the maximum impedance sensitivity is  $-343.37 \Omega/\text{Hz}$  in dark condition. While the capacitance sensitivity was highest when light intensity was  $325 \text{ W/m}^2$  ( $-37.27 \text{ pF/kHz}$ ), respectively. We attribute these observations due to the generation of electron-hole pairs under light and by the increase of their concentration, by the presence of the built-in capacitance and possible frequency dependence of the mobility of the charges.

### Introduction

Photodetectors play a crucial role in the area of flame sensing, missile plume detection, military, environmental water distillation, real-time measurements, and industrial applications [1]. Instead of high cost, poor selectivity in infrared and visible spectra, high voltage and vacuum requirement optical sensors based on inorganic semiconductor materials are available in the market due to a great advantage of quick response [2–4]. To overcome these disadvantages hybrid organic-inorganic perovskites are the best material for fabrication of photodetectors [5–8]. The bandgap of these synthesized organometallic halide perovskites material is tunable and showed high performances as

light-emitting diodes, field-effect transistors, photodetectors, sensors, waveguides and modulators [9–18]. Non-linear properties of 0D/2D perovskite have been also studied widely in literature and its utilization in ultrafast optoelectronic communication have been observed [19–21]. In a typical perovskite heterojunction, electron and hole transport layers i.e., ETL and HTL, are used to enhance its absorption efficiency [22–25].

Although perovskite has numerous advantages, its devices are still not commercialized due to its stability issues. However, the lead in perovskite is toxic therefore researchers are working on lead-free perovskite compositions [9,10]. Furthermore, the perovskite degradation due to light, oxygen, moisture etc is the main issue to avoid it either

\* Corresponding authors at: Ghulam Ishaq Khan Institute of Engineering Sciences and Technology, Topi 23640, KPK, Pakistan (N. Fatima). Solar Energy Research Institute, The National University of Malaysia, 43600 Bangi, Selangor, Malaysia (Md. Akhtaruzzaman).

E-mail addresses: [noshinfatima1990@gmail.com](mailto:noshinfatima1990@gmail.com) (N. Fatima), [akhtar@ukm.edu.my](mailto:akhtar@ukm.edu.my) (Md. Akhtaruzzaman).

<https://doi.org/10.1016/j.rinp.2019.102699>

Received 9 August 2019; Received in revised form 23 September 2019; Accepted 23 September 2019

Available online 26 September 2019

2211-3797/ © 2019 The Authors. Published by Elsevier B.V. This is an open access article under the CC BY-NC-ND license

(<http://creativecommons.org/licenses/by-nc-nd/4.0/>).

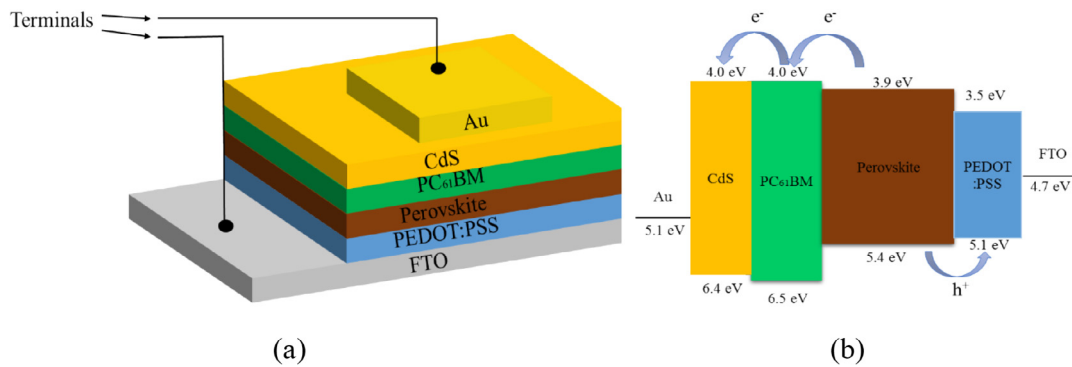


Fig. 1. (a) Schematic view and (b) energy level of perovskite photodetector.

good encapsulation of devices or materials which remain unaffected by these parameters should be selected for the improved results, long term stability and anti-oxidation of perovskite-based devices. The devices degrade rapidly as compare to other photosensitive materials a possible reason can be the poor interface between the substrate and interfacial layers [25,26]. The perovskite is usually paired with PEDOT:PSS, as it has good conductivity, its work function is quite high and can be deposited by an easy technique of solution processing [27]. Literature showed that the perovskite materials band-gap is  $\sim 1.3$  eV which is very good for optical devices [28]. Its highest occupied molecular orbital (HOMO) level is 4.1 eV, while its lowest unoccupied molecular orbital (LUMO) is at 3.7 eV [29]. These materials are also well investigated in the area of solar cells application with narrow band gaps along with their thermal stability [30].

One of the most important areas for utilization of organic semiconductors is the light detectors, which provide many advantages including low cost, high sensitivity, and environment-friendly technology [31,32]. Perovskite-based photodetector, with a complete structure i.e., ITO/PEDOT:PSS/CH<sub>3</sub>NH<sub>3</sub>PbI<sub>2.4</sub>Br<sub>0.6</sub>/PC<sub>61</sub>BM/C<sub>60</sub>/LiF/Ag was fabricated by brush coating and at 650 nm light illumination, a value of  $\sim 1011$  Jones was observed ( $-5$  V biased voltage) [33]. Another photodetector with PEDOT:PSS film was investigated and results showed an increment of work function and resistivity with an increase in light [34]. A perovskite-based optocoupler device was fabricated and light effect showed a sensitivity of  $\sim 10^4$  with the biased voltage of 0–4 V. Although when 6 V is applied at input it achieved photo-responsivity of 1.0 AW<sup>-1</sup> and current transfer ratio about 28.2% and amplified up to 263.3% at 341.3  $\mu$ W cm<sup>-2</sup> [35]. It was concluded that a good selection of sensitive material for photodetectors requires strong absorption, the mobility of charges should be high and convenience between materials energy levels.

In this article, we present results of the light influence on the impedance and capacitance of the photodetector. The perovskite is sandwiched between hole and electron transport layers with the full device structure FTO/PEDOT:PSS/Perovskite/PC<sub>61</sub>BM/CdS/Ag. The photodetector was fabricated by using a low-cost spin coating technology. To enhance the device performance, excitons generation, light absorption and stability of perovskite layer, the cadmium sulfide (CdS) along with PC<sub>61</sub>BM are selected as an electron transport layer (ETL) and PEDOT:PSS as the hole transport layer (HTL) [36,37].

## Experimental

Perovskite (CH<sub>3</sub>NH<sub>3</sub>PbI<sub>3-x</sub>Cl<sub>x</sub>), Poly(3,4-ethylene dioxythiophene): Poly(styrene sulfonate) (PEDOT:PSS), Fullerene derivative [6,6]-phenyl-C<sub>61</sub>-butyric acid methyl ester (PC<sub>61</sub>BM) and Cadmium Sulfide (CdS) were purchased from Ossila.

The photodetector was fabricated in an inert vacuum environment. First of all, the FTO coated glass slides were cleaned sequentially in acetone for 10 min, then for further 10 min, they were cleaned with

ethanol within the ultrasonic bath. Followed by cleaning distilled water and N<sub>2</sub> blower was used to dry the slides and finally processed in plasma etcher for 5 min under 1 mbar pressure. Then to avoid short-circuiting between electrodes the glass substrate with pre-deposited FTO was isolated from sides of slides.

Later, the substrates for 30 min heated on hot the plate at 120 °C and HTL of PEDOT:PSS was spin-coated at 2000 rpm on FTO coated slide for 30 sec. Afterward, it was annealed for 10 min at 130 °C and a layer of perovskite was spin-coated for 30 sec at speed of 3000 rpm, followed by drops of chlorobenzene on perovskite during last 15 sec. Then once again slide was annealed for 90 min at 100 °C, while perovskite film transformed its color from pale yellow to dark brown confirming its layer deposition. After this, the ETL of PC<sub>61</sub>BM (dissolved in chlorobenzene) was spin-coated at 1500 rpm over perovskite film for 30 sec. Moreover, another ETL of 70 nm thick CdS was deposited over PC<sub>61</sub>BM followed by silver as the top electrode through the thermal evaporator at 10<sup>-6</sup> mbar. Schematic diagram of the finalized photodetector is presented in Fig. 1(a). However, Fig. 1(b) shows the energy levels of the device.

During experiments, the samples were placed in the chamber at ambient condition. Devices were fabricated by Laurell WS-650-23NPP spin coater. The light intensity was measured by LM-80 AMPROBE intensity meter. As a light source, the filament lamp was used with the emission spectrum of wavelengths ranging from 200 nm to 850 nm. Impedance and capacitance within the range of frequencies from 100 Hz to 200 kHz were measured by LCR meter MT 4090. Experiments were conducted in cleanroom. JEOL JSM-6460 and Flex AFM Nanosurf 3000 was used for scanning electron and atomic force microscopy. The X-ray diffraction analysis and UV-absorption spectrum were characterized by the Philips PW3710 and Beckman DU640 UV/V spectrophotometer, respectively.

## Results and discussion

The surface morphology of fresh and 90 days aged perovskite is shown in Fig. 2(a) and (b) measured by scanning electron microscope (SEM) at 2  $\mu$ m. The fresh perovskite film grain size is between 150 and 300 nm in diameter and surface is pinhole-free, while the aged samples confirm the degradation of the device and layer shows needle-like structure. Although, the PEDOT:PSS and then perovskite layer on PEDOT:PSS through AFM is shown in Fig. 2(c) and (d). The 3D images reveal that the average roughness of PEDOT:PSS layer is 140 nm, where the average roughness of the perovskite layer is up to 230 nm. It can be perceived that film is well adherent but not free from crystal defects, as the large gran sizes designate roughness of the film which eventually intensifies the series resistance of the device.

For the composition of crystalline structure perovskite (CH<sub>3</sub>NH<sub>3</sub>PbI<sub>3-x</sub>Cl<sub>x</sub>) material was categorized by X-ray diffraction. Fig. 3 (a) ratifies the existence of methylamine lead halide perovskite and its

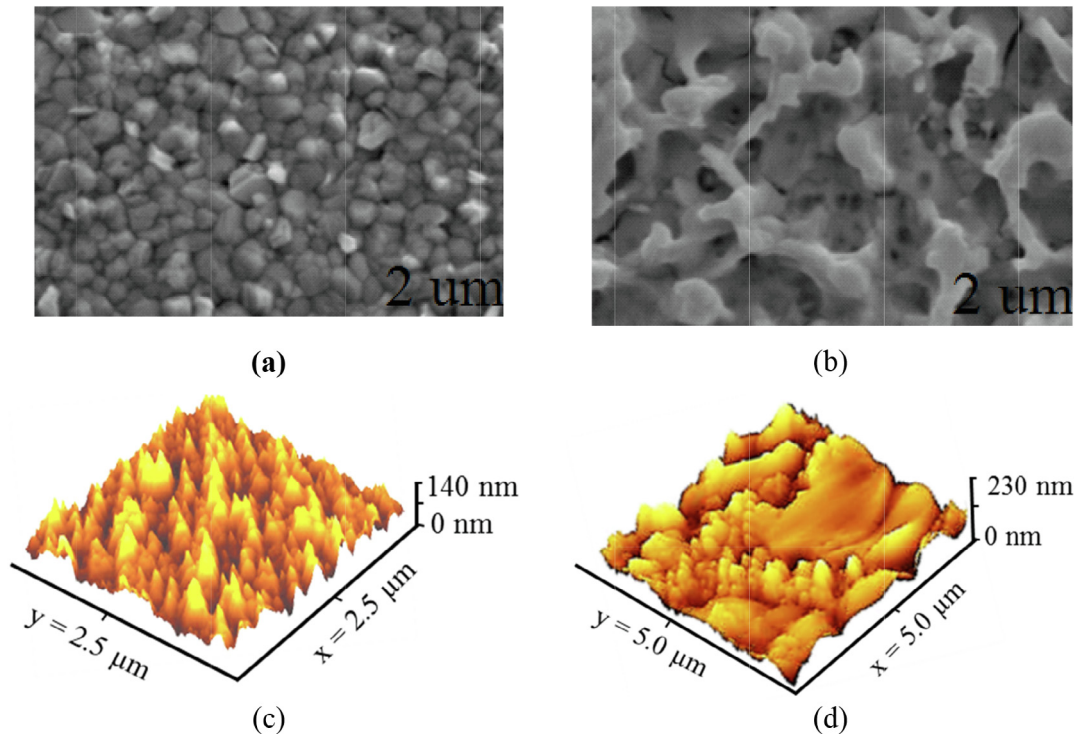


Fig. 2. Shows the SEM image of (a) fresh, (b) 90 days aged perovskite film, and 3D atomic force microscopy of (c) PEDOT:PSS and (d) Perovskite layer over PEDOT:PSS, respectively.

cubic crystal were represented by (2 2 0) and (3 3 0) planes, however, the peaks were observed at 28.4° and 43.1°, respectively. Afterward, the perovskite layer was characterized for the absorption spectrum within ultraviolet and visible range by UV-Vis spectroscopy as presented in Fig. 3(b). The absorption spectrum revealed that the methyl halide perovskite covers the broad spectrum from 350 to 750 nm indicating that its selection in photosensitive applications is appropriate.

The electric characterization of the finalized samples was done and calculated impedance- and capacitance to light intensity relationships at different frequencies. Each of the following sensor's response was measured three times, results were repetitive and graphs are based on averaged data. Fig. 4 shows the dependence of impedance at different frequencies 100 Hz, 1 kHz, 10 kHz, 100 kHz and 200 kHz of FTO/PEDOT:PSS/Perovskite/PC<sub>61</sub>BM/CdS/Ag samples as a function of light intensity. However, with an increment in light intensity, the impedance

decreases and all frequencies follow the same pattern. Although as the frequency increases the graphical results showed that the change in impedance becomes small. Precisely when intensity of light increases, the impedance decrease from 0 to 325 W/m<sup>2</sup> was 2.46 (at 100 Hz), 1.57 (at 1 kHz), 1.09 (at 10 kHz), 1.05 (at 100 kHz) and 1.03 (at 200 kHz) times, respectively.

Fig. 5 presents that under the same physical conditions the sample capacitance was measured. Results show that there is an increment in capacitance of the samples as the light intensity increases from 0 to 325 W/m<sup>2</sup> by factor of 1.301 (at 100 Hz); 1.086 (at 1 kHz); 1.068 (at 10 kHz); 1.063 (at 100 kHz) and 1.062 (at 200 kHz). The dependencies are slightly non-linear at lower frequencies and quasi-linear at higher frequencies.

Under the effect of light intensity the change is either reversible (concerning physical properties) or irreversible (concerning structures)

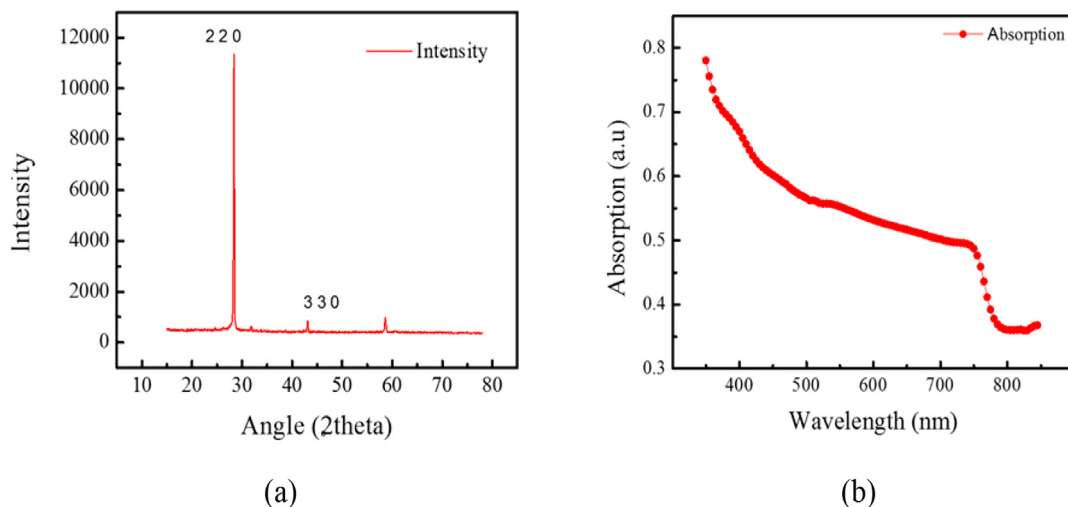


Fig. 3. (a) XRD image and (b) UV-Visible absorption spectrum of perovskite layer.

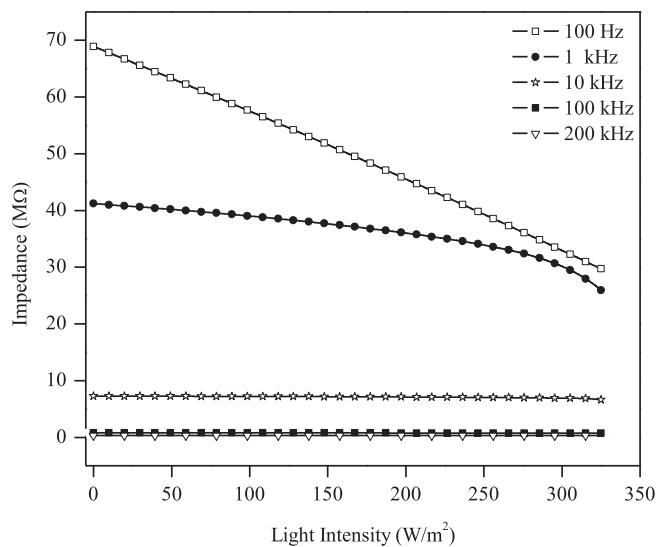


Fig. 4. The impedance-light intensity characterization at varying frequencies of perovskite based samples.

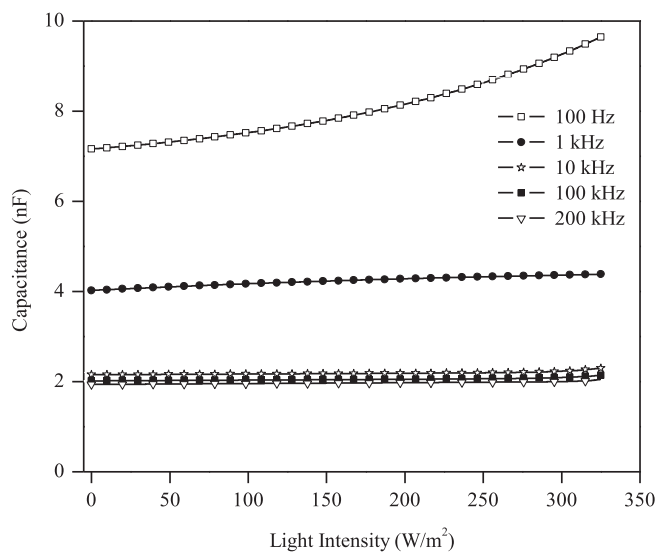


Fig. 5. The capacitance-light intensity characterization at varying frequencies of the perovskite based samples.

process takes place. Our results concerning the characterization of impedance and capacitance w.r.t. light of the FTO/PEDOT:PSS/Perovskite/PC<sub>61</sub>BM/CdS/Ag sensor which can be explained by an increase in the concentration of charges due to generation of the electron-hole pairs. This effect was reversible, probably, due to low concentration of the intensity of light intensity.

The sensitivity ( $S_{Z/G}$  and  $S_{C/G}$ ) is an important parameter that can give us the rate of variation in impedance and capacitance with increasing light intensity. It can be determined by:

$$S_{Z/G} = \frac{\Delta Z}{\Delta G} \quad (1)$$

$$S_{C/G} = \frac{\Delta C}{\Delta G} \quad (2)$$

where  $\Delta Z$ ,  $\Delta C$  and  $\Delta G$  refers to the change in impedance, capacitance and light intensity. Summary Table 1 showed the sensitivity of the light sensor w.r.t. impedance and capacitance.

Our data shows the values of  $S_{Z/G}$  and  $S_{C/G}$  decreased sharply with increase of the applied frequency. The reason could be the presence of

Table 1

Sensitivity under effect of light intensity of perovskite based photodetector with varying frequencies.

Frequency kHz	$S_{Z/G}$ kΩm <sup>2</sup> /W	$S_{C/G}$ pFm <sup>2</sup> /W
0.100	-27.95	265
1	-6.965	17.0
10	-1.290	10.3
100	-0.525	2.20
200	-0.380	1.40

capacitance presented in Eq. (3) and shown in Fig. 6(a). Although, Fig. 6(b) shows the simplified form of the circuit. The perovskite is used as the sensing layer, the parallel combination of capacitance ( $C$ ) and resistance ( $R$ ) can be utilized to model the impedance ( $Z$ ) of the photodetector. Fig. 6 shows the equivalent circuit for the fabricated perovskite-based photodetector [38]. The Fig. 6 presents  $C$  as the sum of both air-filled pores and active film dielectrics while cumulative resistance is shown by  $R$ , acting also as light function represented in Eq. (3) [39].

$$Z = \frac{R}{1 + j\omega RC} \quad (3)$$

where  $\omega$  represents the angular frequency. When there is increment in the charges concentration it effects the permittivity of the materials. In our case with increase in intensity of light, there was decrease in impedance and increase in the capacitance, similar results were also observed in literature [40,41]. The capacitance of the absorbent layer is highly sensitive to its polarizabilities which can be in form of electronic ( $\alpha_e$ ), dipolar ( $\alpha_{dp}$ ) and ionic ( $\alpha_i$ ) [42]. However another type of polarizability is due to transfer ( $\alpha_{tr}$ ) of charge carriers [43,44]. It should be differentiated that  $\alpha_e$  is due to the orbital electron's relative displacement, where  $\alpha_{tr}$  occurs due to charges which participates in process of conduction.

In [42], if only  $\alpha_{tr}$  (due to electrons and holes) is considered, then Clausius-Mosotti relation can be represented as in Eq. (4).

$$\frac{\varepsilon - 1}{\varepsilon + 2} = \frac{N\alpha_{tr}}{3\varepsilon_0} \quad (4)$$

where  $\varepsilon$  is the relative permittivity,  $N$  is the total concentration of charge carriers, and  $\varepsilon_0$  is the permittivity of free space.

Furthermore, the impedance- and capacitance-frequency characteristics were measured at different light intensities and results showed a response in decreasing response of electric parameters as was seen from Eq. (3). Fig. 7. Represents that the impedance of FTO/PEDOT: PSS/Perovskite/PC<sub>61</sub>BM/CdS/Ag samples is dependent on frequency at different intensities of the light. Results shows that with an increment in frequency, the decrease in impedance by a factor of 191.66 (intensity of light = 0), 160.11 (intensity of light = 100), 131.42 (intensity of light = 200), 98.26 (intensity of light = 300), and 80.23 (intensity of light = 325), times observed respectively.

Fig. 8 shows the dependence of the capacitance of the samples on frequency at different intensities of light. It is seen that as frequency increases the capacitance decreases 3.78 (intensity of light = 0), 3.826 (intensity of light = 100), 4.03 (intensity of light = 200), 4.65 (intensity of light = 300) and 4.63 (intensity of light = 325) times. The results showed that in range from 100 Hz to 200 kHz the impedance sensitivity in Ω/Hz is -343.37 (light intensity = 0), -283.36 (light intensity = 100 W/m<sup>2</sup>), -228.36 (light intensity = 200 W/m<sup>2</sup>), -168.35 (light intensity = 300 W/m<sup>2</sup>) and -138.324 (light intensity = 325 W/m<sup>2</sup>), respectively. While the capacitance sensitivity in pF/kHz is -26.86 (light intensity = 0), -27.71 (light intensity = 100 W/m<sup>2</sup>), -30.09 (light intensity = 200 W/m<sup>2</sup>), -36.51 (light intensity = 300 W/m<sup>2</sup>) and -37.27 (light intensity = 325 W/m<sup>2</sup>), respectively.

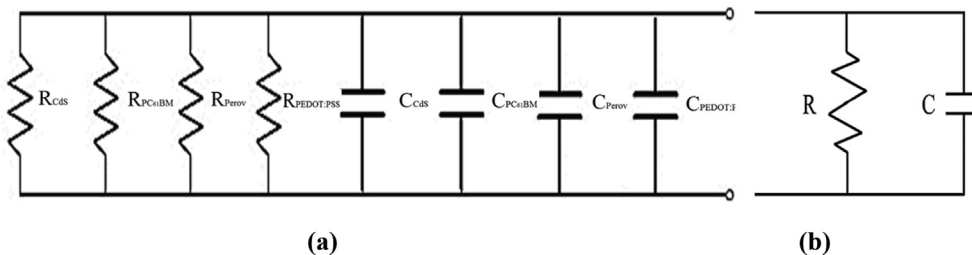


Fig. 6. (a) Equivalent circuit of FTO/PEDOT-PSS/Perovskite/PCBM/CdS/Ag sensor and (b) its simplified.

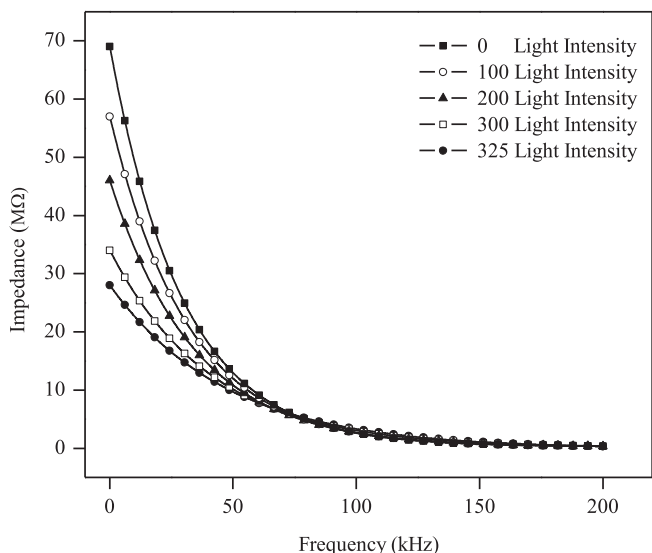


Fig. 7. The dependences of the impedance of the FTO/PEDOT:PSS/Perovskite/PC<sub>61</sub>BM/CdS/Ag samples on frequency at different intensities of light.

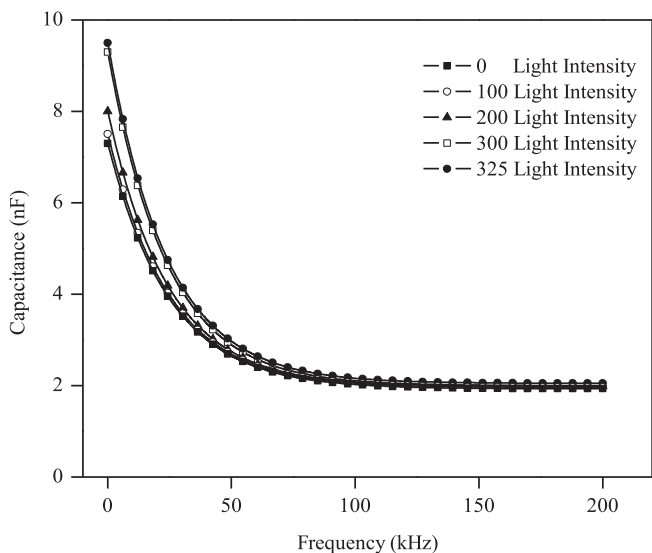


Fig. 8. Capacitance-frequency relationship of FTO/PEDOT:PSS/Perovskite/PC<sub>61</sub>BM/CdS/Ag samples at different light intensities.

The relationships shown in Figs. 7 and 8 can be explained by the increase of the reactive currents through the capacitance with respect to the active current through the resistance. On the other hand, at higher frequencies, the frequency-resistance relationship can be explained by the frequency dependence of the mobility of the charges which was also investigated in Ref. [45]. The sensitivity decreases with the increase of frequency is due to the fact that at lower frequencies charges get time to

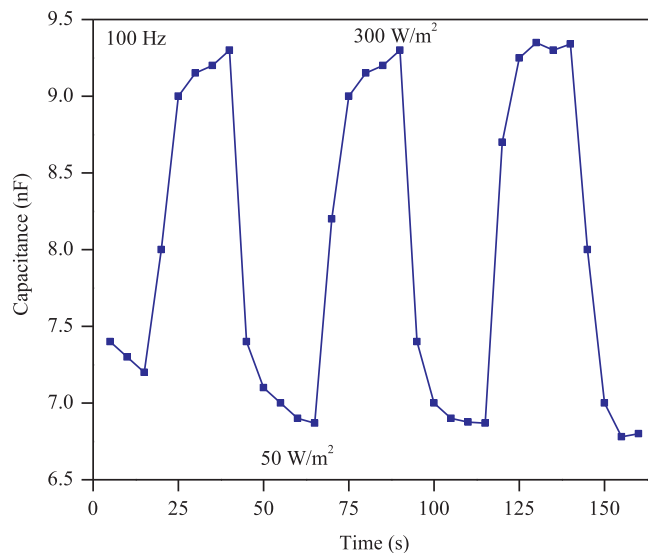


Fig. 9. Capacitive transient response of FTO/PEDOT:PSS/Perovskite/PC<sub>61</sub>BM/CdS/Ag sensor under pulsed light intensities signal (from 50 W/m<sup>2</sup> to 300 W/m<sup>2</sup>) and 100 Hz frequency.

settle down while at higher frequencies the settling time is insufficient, hence as a result sensitivity decreased, respectively. The response and recovery time is 7 sec and 9 sec as observed in Fig. 9.

Perovskite-based solar cell degradation is one of the major issues but if we can utilize these materials for some other applications where their degradation have almost no impact on the electric parameters, then it will help in finding the ways to utilize perovskite materials by one way or other. We hope that the fabrication and investigation of perovskite samples for light sensor will be interesting for different applications in instrumentation and electronics.

### Conclusions

In this work, we described the fabrication and investigation of electric properties on light for perovskite sensor. The sensor has sandwich-surface type structure FTO/PEDOT:PSS/Perovskite/PC<sub>61</sub>BM/CdS/Ag. Investigation of the impedance and capacitance at 100 Hz, 1 kHz, 10 kHz, 100 kHz and 200 kHz of the FTO/PEDOT:PSS/Perovskite/PC<sub>61</sub>BM/CdS/Ag samples. Under effect of light varying from dark condition to 325 W/m<sup>2</sup> showed that there is a decrement in impedance as the photo intensity increased whereas the capacitances of the samples increased. The increase of the frequency of the applied voltage results in a decrease in the impedance and capacitance of the photo-detector.

The change in impedance and capacitance of the samples with the increase of intensity of the light can be explained by generation of the electron-hole pairs and increase of the concentration of charges. These sensors can prove valuable in the field of instrumentation, electronics and photonics.

## Acknowledgments

The authors are thankful to GIK Institute and also to Universiti Kebangsaan Malaysia for supporting this study through the modal Insan grant (MI-2014-14). The authors also extend their appreciation to the deanship of Scientific Research at King Saud University for funding this work through Research group no. RGP-1440-116.

## Declaration of Competing Interest

The authors declare no conflict of interest.

## References

- [1] Stylianakis M, Maksudov T, Panagiotopoulos A, Kymakis E, Kakavelakis G, Petridis K. Inorganic and hybrid perovskite based laser devices: a review. *Preprints* 2019;2019010213 (doi: 10.20944/preprints201901.0213.v1).
- [2] Suzuka M, Uchida R, Matsui T. Photosensor including photoelectric conversion layer containing perovskite compound, and optical detection device including the same. U.S. Patent Application 16/035,593, filed January 24; 2019.
- [3] Chen Y, Zhang X, Liu Z, Zeng Z, Zhao H, Wang X, et al. Light enhanced room temperature resistive NO<sub>2</sub> sensor based on a gold-loaded organic-inorganic hybrid perovskite incorporating tin dioxide. *Microchim Acta* 2019;186(1):47.
- [4] Sun W, Can H, Ruiqin F, Shuai L, Yujie W, Yun-Feng X, et al. On-chip-integrated methylammonium halide perovskite optical sensors. *Adv Opt Mater* 2019;7(6):1801308.
- [5] Zhang Y, Lim CK, Dai Z, Yu G, Haus JW, Zhang H, et al. Photonics and optoelectronics using nano-structured hybrid perovskite media and their optical cavities. *Phys Rep* 2019.
- [6] Snaith HJ. Perovskites: the emergence of a new era for low-cost, high-efficiency solar cells. *J Phys Chem Lett* 2013;4:3623–30.
- [7] Grinberg I, West DV, Torres M, Gou G, Stein DM, Wu L, et al. Perovskite oxides for visible-light-absorbing ferroelectric and photovoltaic materials. *Nature* 2013;503(7477):509–12.
- [8] Kazim S, Nazeeruddin MK, Grätzel M, Ahmad S. Perovskite as light harvester: a game changer in photovoltaics. *Angew Chem Int Ed* 2014;53:2812–24.
- [9] Ju D, Xiaomei J, Hang X, Xi C, Xiaobo H, Xutang T. Narrow band gap and high mobility of lead-free perovskite single crystal Sn-doped MA<sub>3</sub>Sb<sub>2</sub>I<sub>9</sub>. *J Mater Chem A* 2018;6(42):20753–9.
- [10] Zhu W, Shen C, Wu Y, Zhang H, Li E, Zhang W, et al. Semi-locked tetrathienylethene as promising building block for hole transporting materials: toward efficient and stable perovskite solar cells. *Angew Chem Int Ed* 2019. <https://doi.org/10.1002/anie.201811593>.
- [11] Singh DK, Manam J. Efficient dual emission mode of green emitting perovskite BaTiO<sub>3</sub>: Er<sup>3+</sup> phosphors for display and temperature sensing applications. *Ceram Int* 2018;44(9):10912–20. <https://doi.org/10.1016/j.ceramint.2018.03.151>.
- [12] Cerdà J, Arbiol J, Dezanneau G, Diaz R, Morante JR. Perovskite-type BaSnO<sub>3</sub> powders for high temperature gas sensor applications. *Sens Actuat B: Chem* 2002;84(1):21–5. [https://doi.org/10.1016/s0925-4005\(02\)00005-9](https://doi.org/10.1016/s0925-4005(02)00005-9).
- [13] Stambolova I, Konstantinov K, Vassilev S, Peshev P, Tsacheva T. Lanthanum doped SnO<sub>2</sub> and ZnO thin films sensitive to ethanol and humidity. *Mater Chem Phys* 2000;63(2):104–8.
- [14] Zhao X, Liu S, Zhang H, Chang S-Y, Huang W, Zhu B, et al. 20% Efficient perovskite solar cells with 2d electron transporting layer. *Adv Funct Mater* 2019;29(4):1805168.
- [15] Lotsch BV. New light on an old story: perovskites go solar. *Angew Chem Int Ed* 2014;53:635–7.
- [16] Mitzi DB. Synthesis, structure, and properties of organic-inorganic perovskites and related materials. *Prog Inorg Chem* 2007;48:1–121.
- [17] Li P, Chen Y, Yang T, Wang Z, Lin H, Xu Y, et al. Two-dimensional CH<sub>3</sub>NH<sub>3</sub>PbI<sub>3</sub> perovskite nanosheets for ultrafast pulsed fiber lasers. *ACS Appl Mater Interf* 2017;9(14):12759–65.
- [18] Qi X, Zhang Y, Ou Q, Ha ST, Qiu CW, Zhang H, et al. Photonics and optoelectronics of 2D metal-halide perovskites. *Small* 2018;14(31):1800682.
- [19] Wang Y, Chen K, Hao H, Yu G, Zeng B, Wang H, et al. Engineering ultrafast charge transfer in a bismuthene/perovskite nanohybrid. *Nanoscale* 2019;11(6):2637–43.
- [20] Ou Q, Zhang Y, Wang Z, Yuwono JA, Wang R, Dai Z, et al. Strong depletion in hybrid perovskite p-n junctions induced by local electronic doping. *Adv Mater* 2018;30(15):1705792.
- [21] Zhang Y, Lim CK, Dai Z, Yu G, Haus JW, Zhang H, et al. Photonics and optoelectronics using nano-structured hybrid perovskite media and their optical cavities. *Phys Rep* 2019;795:1–51.
- [22] Burschka J, Pellet N, Moon SJ, Humphry-Baker R, Gao P, Nazeeruddin MK, et al. Sequential deposition as a route to high-performance perovskite-sensitized solar cells. *Nature* 2013;499(7458):316–9.
- [23] Jeon NJ, Noh JH, Yang WS, Kim YC, Ryu S, Seo J, et al. Compositional engineering of perovskite materials for high-performance solar cells. *Nature* 2015;517(7535):476–80.
- [24] Docampo P, Hanusch FC, Stranks SD, Doblinger M, Feckl JM, Ehrensperger M, Minar NK, Johnston MB, Snaith HJ, Bein T. Solution deposition-conversion for planar heterojunction mixed halide perovskite solar cells. *Adv Energy Mater* 2014;4(14):1400355.
- [25] Eperon GE, Burlakov VM, Docampo P, Goriely A, Snaith HJ. Morphological control for high performance, solution-processed planar heterojunction perovskite solar cells. *Adv Funct Mater* 2014;24:151–7.
- [26] Liu D, Kelly TL. Perovskite solar cells with a planar heterojunction structure prepared using room-temperature solution processing techniques. *Nat Photonics* 2014;8:133–8.
- [27] Mei A, Li X, Liu L, Ku Z, Liu T, Rong Y, et al. A hole-conductor-free, fully printable mesoscopic perovskite solar cell with high stability. *Science* 2014;345(6194):295–8.
- [28] Yang TC-J, Fiala P, Jeangros Q, Ballif C. High-bandgap Perovskite materials for multijunction solar cells. *Joule* 2018;2(8):1421–36. <https://doi.org/10.1016/j.joule.2018.05.008>.
- [29] Schulz P, Edri E, Kirmayer S, Hodes G, Cahen D, Kahn A. Interface energetics in organo-metal halide perovskite-based photovoltaic cells. *Energy Environ Sci* 2014;7(4):1377–81. <https://doi.org/10.1039/c4ee00168k>.
- [30] Yang Z, Rajagopal A, Jen AK-Y. Ideal bandgap organic-inorganic hybrid perovskite solar cells. *Adv Mater* 2017;29(47):1704418. <https://doi.org/10.1002/adma.201704418>.
- [31] Su Z, Li W, Chu B, Li T, Zhu J, Zhang G, et al. High response organic ultraviolet photodetector based on blend of 4, 4', 4''-tri-(2-methylphenyl phenylamino) triphenylamine and tris-(8-hydroxyquinoline) gallium. *Appl Phys Lett* 2008;93(10):334.
- [32] Tian W, Zhou H, Li L. Hybrid organic-inorganic perovskite photodetectors. *Small* 2017;13(41):1702107. <https://doi.org/10.1002/sml.201702107>.
- [33] Xiang S, Dong S, Huang J. Organic-inorganic hybrid perovskite photodetectors achieved via brush-coating process. 9th International symposium on advanced optical manufacturing and testing technologies: subdiffraction-limited plasmonic lithography and innovative manufacturing technology, T, 10842. International Society for Optics and Photonics; 2019. p. 108420. <https://doi.org/10.1117/12.2506449>.
- [34] Li HG, Wu G, Shi MM, Chen HZ, Wang M. Synthesis of solution processable ultraviolet sensitive organic molecules and their application in hybrid UV photodetector. *Synth Met* 2010;160(15–16):1648–53.
- [35] Li D, Dong G, Li W, Wang L. High performance organic-inorganic perovskite-optocoupler based on low-voltage and fast response perovskite compound photodetector. *Sci Rep* 2015;5:7902.
- [36] Ananthakumar S, Kumar JR, Babu SM. Cesium lead halide (CsPbX<sub>3</sub>, X = Cl, Br, I) perovskite quantum dots-synthesis, properties, and applications: a review of their present status. *J Photonics Energy* 2016;6(4):042001.
- [37] Song Z, Waththage SC, Phillips AB, Heben MJ. Pathways toward high-performance perovskite solar cells: review of recent advances in organo-metal halide perovskites for photovoltaic applications. *J Photonics Energy* 2016;6(2):022001.
- [38] Nahar RK, Khanna VK. A study of capacitance and resistance characteristics of an Al<sub>2</sub>O<sub>3</sub> humidity sensor. *Int J Electron Theor Exp* 1982;52:557–67.
- [39] Dally JW, Riley W, McConnell KG. Instrumentation for engineering and measurements. New York: John Wiley & Sons; 1983.
- [40] Shah M, Karimov KS, Sayyad M. Organic semiconductor nickel phthalocyanine-based photocapacitive and photosensitive detector. *Semicond. Sci. Technol.* 2010;7:25075014.
- [41] Karimov Khs, Qazi I, Draper PH, Khalid FA, Mahroof-Tahir M, Khan TA. *Environ. Monit. Assess* 2008;141:323–8.
- [42] Omar MA. Elementary solid state physics: principles and applications. Pearson Education (Singapore) Pte. Ltd.; 2002.
- [43] Iwamoto M, Manaka T. Experimental evidence of surface polarization in organic films and control of current-voltage characteristics by the surface polarization. *Proc. Int. Symp. Super-Functionality Organic Devices, IPAP Conf. Series*, 6. 2005. p. 63–8.
- [44] Amy F, Chan C, Kahn A. Polarization at the gold/pentacene interface. *Org Electron* 2005;6:85–91.
- [45] Docampo P, Hanusch FC, Stranks SD, Doblinger M, Feckl JM, Ehrensperger M, Minar NK, Johnston MB, Snaith HJ, Bein T. Solution deposition-conversion for planar heterojunction mixed halide perovskite solar cells. *Adv Energy Mater* 2014;4(14):382–6.